

Bimetallic-MOF Catalyst for Efficient CO₂ Photoreduction from Simulated Flue Gas to Value-added Formate

*Shao-Hong Guo,^{†,‡} Xiang-Juan Qi,[†] Hui-Min Zhou,[†] Jie Zhou,[†] Xiao-Hui Wang,[†] Man Dong,[†]
Xue Zhao,[†] Chun-Yi Sun,^{*,†} Xin-Long Wang,^{*,†} Zhong-Min Su^{†,‡}*

[†]Key Laboratory of Polyoxometalate Science of Ministry of Education, National & Local United Engineering Laboratory for Power Battery, Department of Chemistry, Northeast Normal University, No. 5268 Renmin Street, Changchun, Jilin Province, China

[‡]College of Chemistry, Jilin University, Changchun, Jilin Province, China

***Correspondence to:** *E-mail: wangxl824@nenu.edu.cn; suncy009@nenu.edu.cn

Table of content

Experimental Procedures and DFT Calculations	S3
Results and Discussion	S8

Experimental Procedures and DFT Calculations

1. Experimental section

1.1 Materials

2,5-dioxido-1,4-benzenedicarboxylate (H_4DOBDC), $Ni(CH_3COO)_2 \cdot 4H_2O$ (AR, 99%), $Mg(CH_3COO)_2 \cdot 4H_2O$ (AR, 99%), $Mg(NO_3)_2 \cdot 6H_2O$ (AR, 99%) were purchased from Aladdin. N,N-dimethyl formamide (DMF, AR), methanol (MeOH, AR), deionized water (H_2O), acetonitrile (CH_3CN , GR), triethanolamine (TEOA, AR). All solvents and metal salts were used as received.

1.2 Synthesis

Preparation of bimetallic MOF-74 using a modified method from a previous literature.¹

Take $Ni_{0.75}Mg_{0.25}$ -MOF-74 with the feeding ratio 0.2 : 0.8 of Ni/Mg as an example. H_4DOBDC (148.6 mg, 0.75 mmol), $Ni(CH_3COO)_2 \cdot 4H_2O$ (99.5 mg, 0.4 mmol) and $Mg(CH_3COO)_2 \cdot 4H_2O$ (128.6 mg, 1.6 mmol) were placed into a glass flask and dissolved in 50 mL H_2O . The homogeneous solution was dispensed into 100 mL vial. The vial was sealed with a Teflon-lined cap and placed into an oven heated at 175 °C maintaining for 12 hours. After the vial was allowed to cool to room temperature, the mother liquor was decanted from the vial and the product was cleaned with methanol until completely removing the unreacted reactants. The material was then activated at 200 °C under Ar atmosphere for 8 hours to remove solvents and stored for the further use. Ni-MOF-74 and $Ni_{0.87}Mg_{0.13}$ -MOF-74 with the feeding ratio 0.3 : 0.7 of Ni/Mg were prepared with the similar method.

Preparation of Mg-MOF-74 using a slightly modified method from a previous literature.²

H_4DOBDC (90.00 mg, 0.45 mmol) was placed into a glass flask and dissolved in 30 mL DMF. $Mg(NO_3)_2 \cdot 6H_2O$ (369.22 mg, 1.44 mmol) was put into another glass flask dissolved with 3.6 mL (1:1, v/v) EtOH/ H_2O . These two resulting mixtures were thoroughly mixed with a magnetic stir bar until dissolution of the solids was complete. The homogeneous solution was dispensed into 50 mL vial. The vial was sealed with a Teflon-lined cap and placed into an oven heated at 120 °C maintaining for 24 hours. After the vial was allowed to cool to room temperature, the mother liquor was decanted from the vial and the product was cleaned with DMF every 5 hours until completely removing the unreacted reactants. The precipitation was immersed in the 50 mL fresh MeOH for 7 times over 7 days. After solvent exchange, the material was activated at 250 °C under Ar for 8 hours until dry and stored for the further use.

1.3 Materials characterization

The powder X-ray diffraction patterns (PXRD) are recorded on a SmartLab X-ray diffractometer. The morphology and the energy dispersive X-ray spectroscopy is investigated on transmission electron microscope (TEM) (JEM-2100Plus). The gas sorption measurements are performed on automatic volumetric adsorption equipment. The samples are activated by heating under Ar atmosphere at 200 °C for 8 h before adsorption measurements. After activation, the samples are tested for CO₂ measurements. The absorption behaviors of the samples are studied by the UV-vis spectrometer (Shimadzu UV-2600). UV-vis absorption and diffuse reflection spectroscopy (DRS) is obtained on U-3010 spectrophotometer (Hitachi, Japan). Photoluminescence (PL) spectra are scanned on a photoluminescence spectrometer (Hitachi F-4600) under an excitation wavelength of 520 nm. The luminescent decay curves are recorded on an Edinburgh FSP920 spectrometer equipped with a photomultiplier (PMT), in conjunction with a nanosecond optical parametric oscillator (OPO) pumped by a 480-nm-pulsed laser as the excitation source. I-t curves and Mott-Schottky plots are tested at CHI660e (CH Instruments, Inc., USA) electrochemical workstation. The inductively coupled plasma mass spectrometry (ICP-MS) is performed on the Thermo Scientific Xseries 2. Photographs of MOF crystals are obtained from the microscope of olympus SZX7. The products of photocatalytic reaction are tested by GC-9800 spectrometer and ICS-1000 ion chromatography. The HP 6890GC-5973MSD gas chromatography-mass spectrometer (GC-MS) and ¹³C NMR are employed to analyze the ¹³CO and H¹³COO⁻ generated from the ¹³CO₂ (98% enriched) isotope experiments. All the measurements are performed at room temperature unless otherwise noted.

1.4 Electrochemistry measurements

Fabrication of the MOF-74 photoelectrodes. The ITO substrate was cleaned by sonicating sequentially in deionized water, alcohol and acetone, each for 10 min. The ITO substrate were divided into the size of approximately 1 cm x 1 cm. And 40 μL MOF-74 MeOH suspension (6 mg/mL) was subsequently dropped onto the ITO substrate. The as-prepared photoelectrodes were subsequently dried at room temperature overnight.

I-t curves. The photoelectrochemical characterizations were performed on the electrochemical workstation with a three-electrode configuration with the assembled photoelectrodes as the working electrode, the Pt mesh as the counter electrode and the Ag/AgCl (in 3 M KCl) as the reference electrode. A 0.2 M Na₂SO₄ aqueous solution was filled

in the cell as the electrolyte. The light source and the light density were identical with that in the photocatalytic CO₂ reduction test.

Mott-Schottky analysis. The photoelectrochemical characterizations were performed on the electrochemical workstation with a three-electrode configuration using the assembled photoelectrodes as the working electrode, Pt as counter electrode and 0.2 M Na₂SO₄ as electrolyte. The test was measured at frequencies of 500 Hz, 1000 Hz and 1500 Hz.

1.5 Photocatalytic reaction

Photocatalytic performance in pure CO₂ condition. The photocatalytic CO₂ reduction was conducted in a homemade 50 mL sealed cell with 3 mg Ni_{0.75}Mg_{0.25}-MOF-74 as the catalysts, 7 mg [Ru(bpy)₃]Cl₂ (bpy = 2,2'-bipyridine) as photosensitizer, 5 mL CH₃CN as the solvent and 1 mL TEOA as the sacrificial reagent. Before reduction, high purity CO₂ (99.99%) gas bubbled in the CH₃CN solvent for around 20 min until the CO₂ concentration reached saturation and dissolved oxygen was removed completely. A 300 W Xenon lamp with a 420 nm cutoff filter was used as the light source. The distance between the homemade sealed cell and the 300 W xenon lamp is about 8 cm and the sample geometry of irradiation was about 2 cm × 3 cm. The light intensity was around 200 mW/cm². All of the experiments were carried out under ambient pressure and the reaction system was kept at 20 °C under a cooling water system for 0.5 h. The gaseous products generated during CO₂ photocatalytic reduction were collected by a 1 mL syringe and then immediately analyzed by GC-9800 equipped with a flame ionization detector (FID), and a thermal conductivity detector (TCD) after 0.5 h. The supernatant was diluted 25 folds and used to measure HCOO⁻ by ICS-1000 ion chromatography.

Photocatalytic performance in diluted CO₂ conditions (20%, 15%, 5%). Take 5% CO₂/Ar system as an example. The photocatalytic CO₂ reduction was conducted in a homemade 50 mL sealed cell with 3 mg Ni_{0.75}Mg_{0.25}-MOF-74 as the catalysts, 7 mg [Ru(bpy)₃]Cl₂ (bpy = 2,2'-bipyridine) as photosensitizer, 5 mL CH₃CN as the solvent and 1 mL TEOA as the sacrificial reagent. Before reduction, high purity Ar (99.99%) gas bubbled in the CH₃CN solvent for around 20 min until the dissolved oxygen was removed completely. Then, the diluted 5% CO₂/Ar mixed gas was input into this system for about 15 seconds at a flow rate of 80 mL/min. The resulted 5% CO₂/Ar diluted reaction system was irradiated by a 300 W Xenon lamp with a 420 nm cutoff filter. The distance between the homemade sealed cell and the 300 W xenon lamp is about 8 cm and the sample geometry of irradiation was about 2 cm × 3 cm. The light intensity was around 200 mW/cm². All of the experiments were carried out under ambient pressure and the reaction system was kept at 20 °C under a cooling water system for 0.5 h. The gaseous products generated during CO₂ photocatalytic reduction were collected by a 1

mL syringe and then immediately analyzed by GC-9800 equipped with a flame ionization detector (FID), and a thermal conductivity detector (TCD) after 0.5 h. The supernatant was diluted 25 folds and used to measure HCOO^- by ICS-1000 ion chromatography. The other diluted reaction (20% and 15%) conditions were prepared by the similar method. Photocatalytic experiment in diluted 5% CO_2 condition over Ni-MOF-74 is similar to the above operation.

Photocatalytic performance in simulated flue gas (20% CO_2 + 0.2% H_2S + 0.2% NO_x + 0.2% SO_x). The photocatalytic CO_2 reduction was conducted in a homemade 50 mL sealed cell with 3 mg $\text{Ni}_{0.75}\text{Mg}_{0.25}$ -MOF-74 as the catalysts, 7 mg $[\text{Ru}(\text{bpy})_3]\text{Cl}_2$ (bpy = 2,2'-bipyridine) as photosensitizer, 5 mL CH_3CN as the solvent and 1 mL TEOA as the sacrificial reagent. Before reduction, high purity N_2 (99.99%) gas bubbled in the CH_3CN solvent for around 20 min until the dissolved oxygen was removed completely. Then, the diluted 20% CO_2/N_2 mixed gas was input into this system for about 1 min at a flow rate of 80 mL/min. 0.1 mL H_2S , 0.1 mL NO_x and 0.1 mL SO_x were injected into this system. The obtained reaction system was irradiated by a 300 W Xenon lamp with a 420 nm cutoff filter. The distance between the homemade sealed cell and the 300 W xenon lamp is about 8 cm and the sample geometry of irradiation was about 2 cm × 3 cm. The light intensity was around 200 mW/cm². All of the experiments were carried out under ambient pressure and the reaction system was kept at 20 °C under a cooling water system for 0.5 h. The gaseous products generated during CO_2 photocatalytic reduction were collected by a 1 mL syringe and then immediately analyzed by GC-9800 equipped with a flame ionization detector (FID), and a thermal conductivity detector (TCD) after 0.5 h. The supernatant was diluted 25 folds and used to measure HCOO^- by ICS-1000 ion chromatography. Note that gases of H_2S , NO_x and SO_x are prepared by adding an appropriate amount of sulfuric acid to Na_2S , NaNO_2 and NaHSO_3 , respectively.

Isotopic experiment. The isotopic experiment was conducted in a homemade 50 mL sealed cell with 3 mg $\text{Ni}_{0.75}\text{Mg}_{0.25}$ -MOF-74 crystals as the catalysts, 5 mL CH_3CN as the solvent and 1 mL TEOA as the sacrificial reagent. Before reduction, $^{13}\text{CO}_2$ (98%) gas bubbled in the reaction system for around 20 min until the dissolved oxygen was removed completely. A 300 W xenon lamp with a 420 nm cutoff filter was used as the light source. After 0.5 h, the ^{13}C -labeled products, ^{13}CO and $\text{H}^{13}\text{COO}^-$, were tested by GC-MS and ^{13}C NMR, respectively.

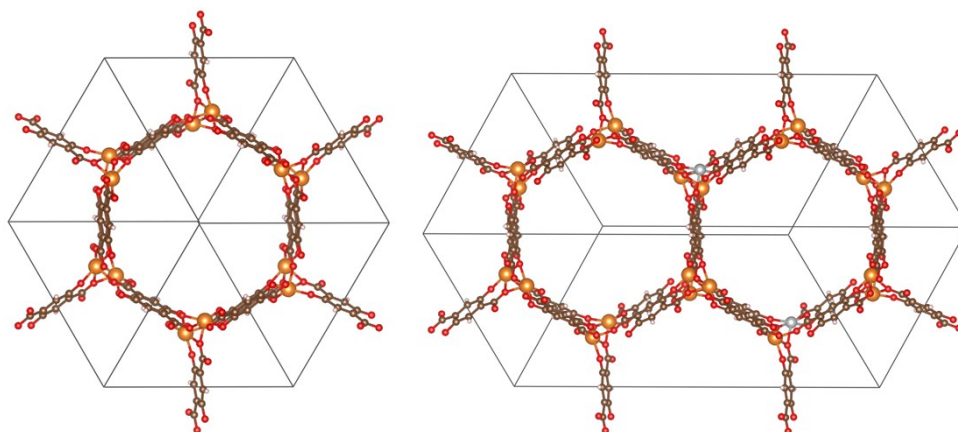
2. DFT Calculations

All the calculations are performed within the framework of DFT implemented in the Vienna ab initio simulation package (VASP).³⁻⁵ The generalized gradient approximation with the

functional is described by the Perdew-Burke-Ernzerhof type (PBE).⁶ The projector-augmented wave (PAW) method⁷ is applied to describe the wavefunctions in the core regions, while the valence wavefunctions are expanded as linear combination of plane-waves with a cutoff energy of 400 eV. The total energy is converged to 10^{-5} eV in the geometry optimizations, and the Hellmann–Feynman force on each relaxed atom is less than 0.01 eV/Å. The effect of Van der Waals (vdW) interactions was also considered by using DFT-D2 scheme.^{8,9} We applied computational hydrogen electrode (CHE) model to analyze the reaction processes from thermodynamics perspective,¹⁰ no transition state search is performed. At $U = 0$ V versus RHE, protons and electrons are at equilibrium with H_2 at 101325 Pa, 298 K, and all pH values. At a given applied potential $U \neq 0$ V versus RHE, the chemical potential of a proton and electron pair can be written as: $\mu(H^+) + \mu(e^-) = \frac{1}{2}\mu(H_2) - eU$, where e is the (positive) electron charge.

For instance, for the first hydrogenation process at an electrode potential U , the reaction energy is: $\Delta E = \mu(COOH^*) - \mu(CO_2^*) - \frac{1}{2}\mu(H_2) - eU$.

The unit cell of MOF-74 contains 54 atoms, the calculations of the CO_2 reduction processes of purely MOF-74 (Ni and Mg) are also based on the finite unit sizes. When the mixing system is considered, we extend the unit cell by 2×1 as shown in the following Figure, which contains 108 atoms.



Computational models (unit cells) for Mg-MOF-74 (left side) and mixed Ni/Mg MOF-74 (right side).

Results and Discussion

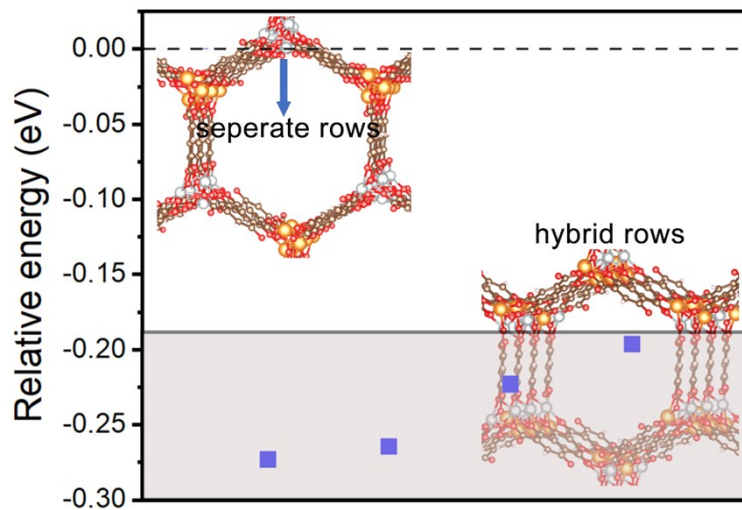


Figure S1. Calculated relative energies of the hybrid Ni/Mg-MOF-74 structures with a Mg:Ni ratio of 1:1, the reference configuration of Mg and Ni in completely separated rows is set to 0.0 eV.

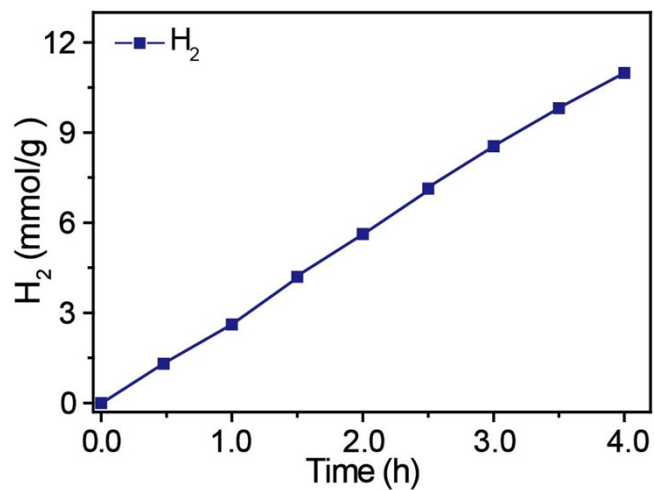


Figure S2. Time-course profile of H₂ catalyzed by Ni_{0.75}Mg_{0.25}-MOF-74.

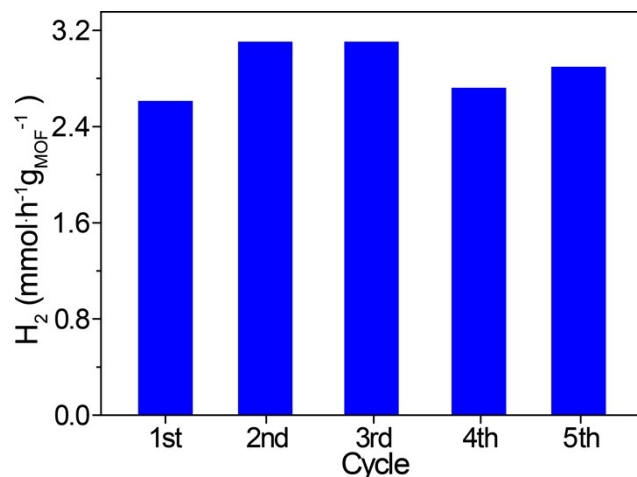


Figure S3. Recyclability of Ni_{0.75}Mg_{0.25}-MOF-74 photocatalyst in five consecutive runs. Catalysts were recovered after each cycle and reused under the same condition.

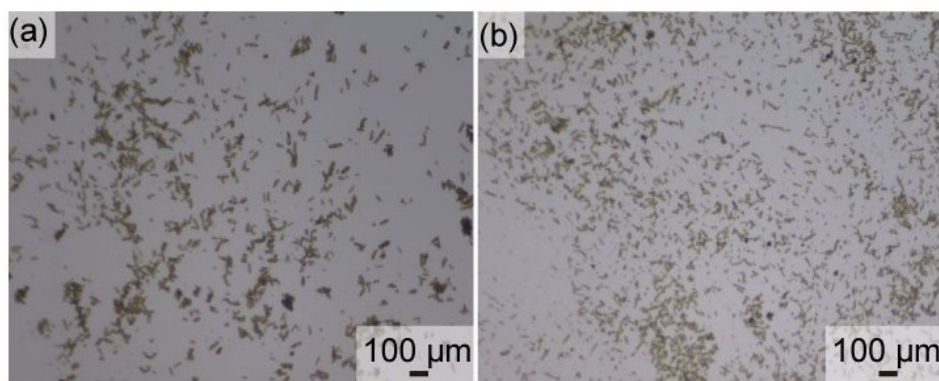


Figure S4. Photographs of the Ni_{0.75}Mg_{0.25}-MOF-74 under the microscope (a) before and (b) after the reduction reaction.

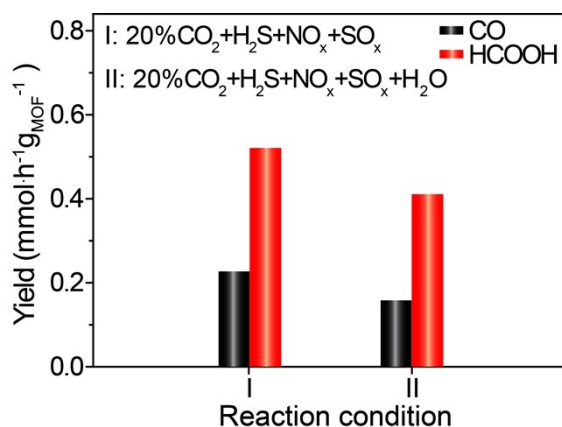


Figure S5. CO₂ photoreduction performance over Ni_{0.75}Mg_{0.25}-MOF-74 in simulated flue gas with 7% H₂O (vapor), 0.2% H₂S, 0.2% NO_x and 0.2% SO_x in 20% CO₂/N₂ system.

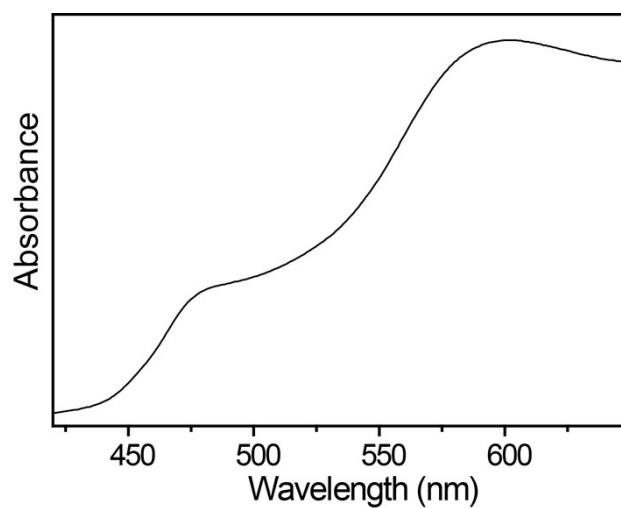


Figure S6. UV-Vis diffusion spectrum of $\text{Ni}_{0.75}\text{Mg}_{0.25}\text{-MOF-74}$.

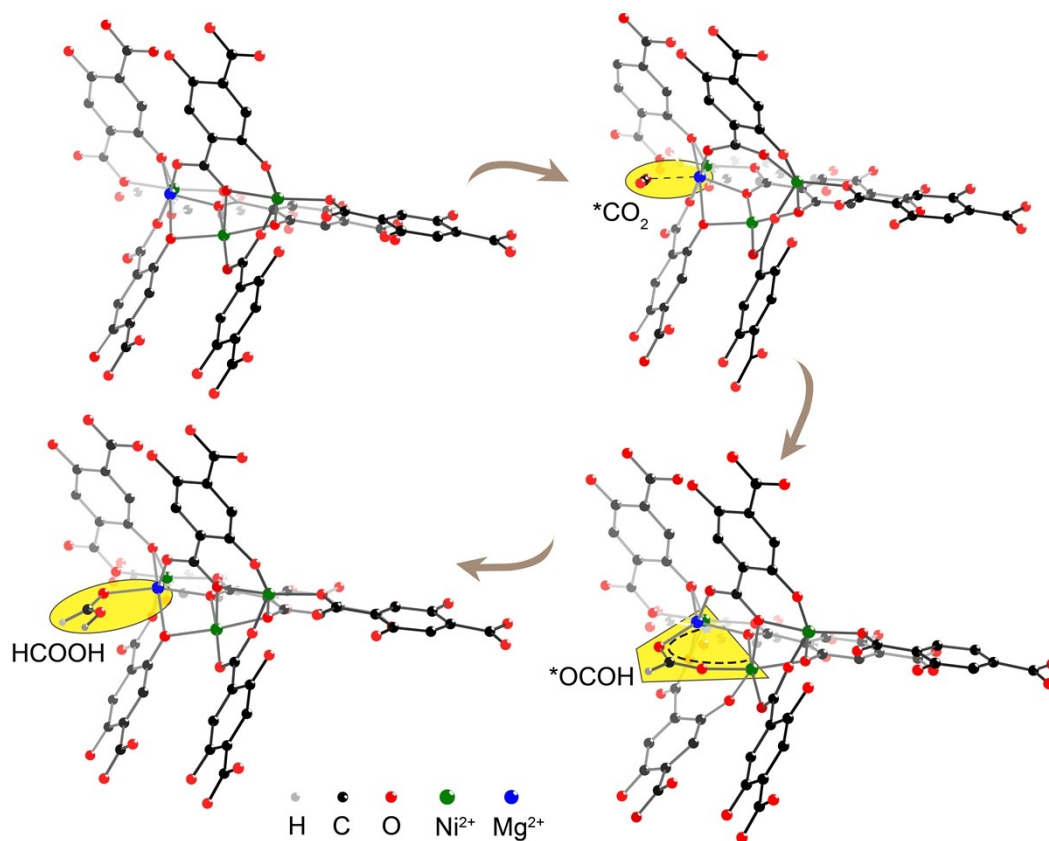


Figure S7. DFT-derived CO_2 binding structures of $\text{Ni}_{0.75}\text{Mg}_{0.25}\text{-MOF-74}$ to generate formate.

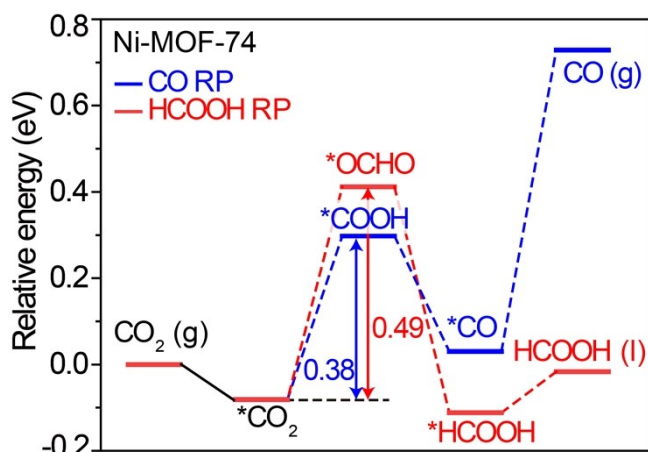


Figure S8. Calculated energy diagram for CO₂ photoreduction based on Ni-MOF-74. RP: reaction path.

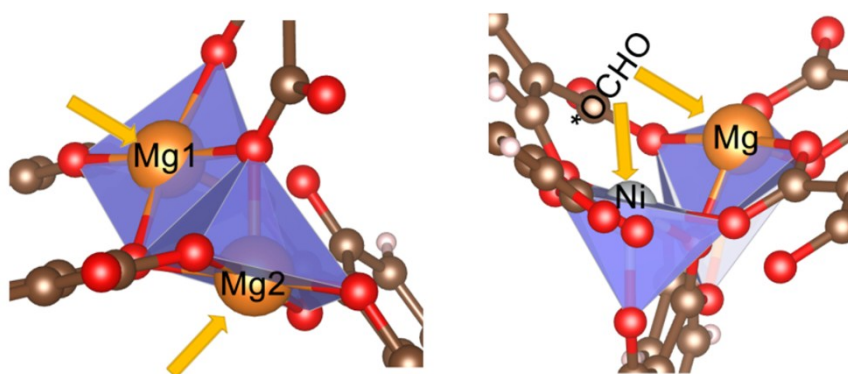


Figure S9. Geometry structures of monometallic Mg-MOF-74 (left side) and mixed Ni-Mg framework in polyhedral style.

In the Mg-MOF-74 structure as shown in **Fig. S9**, the exposed Mg1 and Mg2 sites are in completely different planes and directions. Therefore, the formation of bridge structure on Mg-MOF-74 seems to be unlikely. To verify this, we build a model structure to obtain the bridge structure of Mg-MOF-74, but the geometry falls back to a singly adsorbed *OCHO structure after the geometry optimization procedure, due to the steric effect as we expected. In contrast, the incorporation of Ni atoms can lead to a local structure distortion, which helps to stabilizing the bridge structure. We also attribute the phenomenon to the polarization effect by Ni-O-Mg bond.

Table S1. The photocatalytic performance using Ni_xMg_{1-x}-MOF-74 (x = 1, 0.87, 0.75, 0) as catalyst for CO₂ reduction for 0.5 h irradiation.

Catalyst	HCOO ⁻ (mmol·h ⁻¹ g _{MOF} ⁻¹)	CO (mmol·h ⁻¹ g _{MOF} ⁻¹)	H ₂ (mmol·h ⁻¹ g _{MOF} ⁻¹)
Ni-MOF-74	0.29	0.43	2.22
Ni _{0.87} Mg _{0.13} -MOF-74	0.54	0.52	2.24
Ni _{0.75} Mg _{0.25} -MOF-74	0.64	0.46	2.61
Mg-MOF-74	~0	0.32	1.56

Table S2. Comparison of the formate generation rates for CO₂ photoreduction in pure CO₂ using MOF as catalysts.

Catalyst ^[a]	Photosensitizer	Solvent/Sacrificial agent	Light source	HCOO ⁻ (mmol·h ⁻¹ g ⁻¹)	reference
MOF-253-Ru(CO) ₂ Cl ₂	No	MeCN/TEOA	Xe-300 W 420-800 nm	16.8	11
PCN-222	No	MeCN/TEOA	Xe-300 W 420-800 nm	60	12
NH ₂ -UiO-66(Zr)	No	MeCN/TEOA	Xe-500 W 420-800 nm	26.4	13
MIL-125(Ti)-NH ₂	No	MeCN/TEOA	Xe-300 W 420-800 nm	16.3	14
Eu-Ru(phen) ₃ -MOF	No	MeCN/TEOA	Xe-300 W 420-800 nm	94	15
AUBM-4	No	MeCN/TEOA	Xe-150 W 420-800 nm	366	16
AD-MOF-2	No	H ₂ O/TIPA ^[b]	Xe-300 W 420-800 nm	443.2	17
MIL-101(Fe)	No	MeCN/TEOA	Xe-300 W 420-800 nm	147.5	18
Zr-SDCA-NH ₂	No	MeCN/TEOA	Xe-300 W 420-800 nm	39.2	19
Zr-bpdc/RuCO	[Ru(bpy) ₃](PF ₆) ₂	MeCN/TEOA	Xe-300 W 385-740 nm	23	20
Ni _{0.75} Mg _{0.25} -MOF-74	[Ru(bpy) ₃]Cl ₂ ·6H ₂ O	MeCN/TEOA	Xe-300 W 420-800 nm	638	this work

[a] represents the name in the reference. [b] TIPA: triisopropanolamine

Table S3. The photocatalytic performance with and without Mg-MOF-74 for CO₂ reduction with 0.5 h irradiation.

Catalyst	HCOO ⁻ (μ mol)	CO (μ mol)	H ₂ (μ mol)
Without Mg-MOF-74	~0	0.51	3.01
Mg-MOF-74	~0	0.48	2.35

Table S4. The research of experimental conditions in diluted CO₂ for 0.5 h irradiation over Ni-MOF-74 catalyst.

Reaction condition	HCOO ⁻ (mmol·h ⁻¹ g _{MOF-74} ⁻¹)	CO (mmol·h ⁻¹ g _{MOF-74} ⁻¹)	H ₂ (mmol·h ⁻¹ g _{MOF-74} ⁻¹)
100% CO ₂	0.29	0.43	2.22
5% CO ₂ /Ar	0.10	0.12	1.28

According to the experimental results, monometallic Mg-MOF-74 is almost inactive in pure CO₂ reaction system. Therefore, we did not perform catalytic experiments using Mg-MOF-74 under low CO₂ concentrations. To explore the catalytic activity of Ni-MOF-74 at a low CO₂ level, the CO₂ photoreduction is carried out in 5% CO₂/Ar system (**Table S4**). As a result, the products of formate and CO at 5% CO₂/Ar situation only maintain ~34% and ~28% of the reactivity in pure CO₂, respectively, revealing that formate and CO drop a lot at the same time. This may result from relative weak CO₂ adsorption capability for Ni-MOF-74 in a low CO₂ concentration. Meanwhile, compared with Ni/Mg-MOF-74 catalyst, the intermediate of *OCHO for formate product is only adsorbed on a single metal site Ni in Ni-MOF-74 catalyst, resulting in the higher activation energy for the rate-determining step of formate. The results demonstrate the necessity over bimetallic Ni_{0.75}Mg_{0.25}-MOF-74 catalyst for the high-yield of formate under low CO₂ levels.

Table S5. The photocatalytic performance using Ni_{0.75}Mg_{0.25}-MOF-74 as a catalyst under low concentrations of CO₂.

Reaction condition	HCOO ⁻ (mmol·h ⁻¹ g _{MOF} ⁻¹)	CO (mmol·h ⁻¹ g _{MOF} ⁻¹)	H ₂ (mmol·h ⁻¹ g _{MOF} ⁻¹)
100% CO ₂	0.64	0.46	2.61
20% CO ₂ /Ar	0.60	0.25	2.70
15% CO ₂ /Ar	0.56	0.15	2.05
5% CO ₂ /Ar	0.53	0.10	1.37

Table S6. The photocatalytic performance using Ni_{0.75}Mg_{0.25}-MOF-74 as a catalyst under simulated flue gas.

Reaction condition	HCOO ⁻ (mmol·h ⁻¹ g _{MOF} ⁻¹)	CO (mmol·h ⁻¹ g _{MOF} ⁻¹)	H ₂ (mmol·h ⁻¹ g _{MOF} ⁻¹)
20% CO ₂ /Ar	0.60	0.25	2.70
20% CO ₂ /N ₂ +0.2% H ₂ S+0.2% NO _x +0.2% SO _x	0.52	0.23	2.40
20% CO ₂ /N ₂ +0.2% H ₂ S+0.2% NO _x +0.2% SO _x +7% H ₂ O	0.41	0.16	3.12

In order to explore the catalytic performance of Ni_{0.75}Mg_{0.25}-MOF-74 in the simulated flue gas with 7% H₂O, 0.2% H₂S, 0.2% NO_x, 0.2% SO_x and 20% CO₂/N₂, we conduct the CO₂ photoreduction under visible-light irradiation for 0.5 h (**Table S6**). The results demonstrate that the low content of water vapor in flue gas has an obvious negative effect on the catalytic activity and the yields of formate and CO are up to 0.41 and 0.16 mmol·h⁻¹g_{MOF}⁻¹, which are a little lower than formate (0.52 mmol·h⁻¹g_{MOF}⁻¹) and CO (0.23 mmol·h⁻¹g_{MOF}⁻¹) under flue gas without water vapor, respectively. The obvious decrease of output may be ascribed to the competitive adsorption between the low content of H₂O (7%) and high concentration of CO₂ (20%).

References

- [1] L. Zou, C.-C. Hou, Z. Liu, H. Pang, Q. Xu, *J. Am. Chem. Soc.* **2018**, *140*, 15393–15401.
- [2] A. R. Millward, O. M. Yaghi, *J. Am. Chem. Soc.* **2005**, *127*, 17998–17999.
- [3] G. Kresse and J. Hafner, *Phys. Rev. B*, 1993, **48**, 13115-13118.
- [4] G. Kresse and J. Furthmüller, *Phys. Rev. B*, 1996, **54**, 11169-11186.

- [5] G. Kresse and J. Furthmüller, *Comput. Mater. Sci.*, 1996, **6**, 15-50.
- [6] J. P. Perdew, K. Burke and M. Ernzerhof, *Phys. Rev. Lett.*, 1996, **77**, 3865-3868.
- [7] P. E. Blöchl, *Phys. Rev. B*, 1994, **50**, 17953-17979.
- [8] S. Grimme, J. Antony, S. Ehrlich and H. Krieg, *J. Chem. Phys.*, 2010, **132**, 154104.
- [9] S. Grimme, *J. Comput. Chem.*, 2006, **27**, 1787-1799.
- [10] D.-R Sun, Y.-H Gao, J.-L. Fu, X.-C. Zeng, Z.-N. Chen, Z.-H. Li, *Chem. Commun.* **2015**, 51, 2645--2648.
- [11] J. K. Nørskov, J. Rossmeisl, A. Logadottir, and L. Lindqvist, *J. Phys. Chem. B* **2004**, 108, 17886-17892.
- [12] H-Q Xu, J-H. Hu, D.-K. Wang, Z.-H. Li, Q. Zhang, Y. Luo, S.-H. Yu, H.-L. Jiang, *J. Am. Chem. Soc.* **2015**, 137, 13440-13443.
- [13] D.-R. Sun, Y.-H. Fu, W.-J. Liu, L. Ye, D.-K. Wang, L. Yang, X.-Z. Fu, Z.-H. Li, *Chem. Eur. J.* **2013**, 19, 14279-14285.
- [14] Y.-H. Fu, H. Yang, R.-F. Du, G.-M. Tu, C.-H. Xu, F.-M. Zhang, M.-H. Fan, W.-D. Zhu, *RSC Adv.* **2017**, 7, 42819–42825.
- [15] Z.-H. Yan, M.-H. Du, J.-X. Liu, S.-Y. Jin, C. Wang, G.-L. Zhuang, X.-J. Kong, L.-S. Long, L.-S. Zheng, *Nat. Commun.* **2018**, 9, 3353.
- [16] M. E. Mahmoud, H. Audi, A. Assoud, T. H. Ghaddar, M. Hmadeh, *J. Am. Chem. Soc.* **2019**, 141, 7115-7121.
- [17] N. Li, J. Liu, J.-J. Liu, L.-Z. Dong, Z.-F. Xin, Y.-L. Teng, Y.-Q. Lan, *Angew. Chem. Int. Ed.* **2019**, 58, 5226-5231.
- [18] D.-K. Wang, R.-K. Huang, W.-J. Liu, D.-R. Sun, Z.-H. Li, *ACS Catal.* **2014**, 4, 4254-4260.
- [19] M.-Y. Sun, S.-Y. Yan, Y.-J. Sun, X.-H. Yang, Z.-F. Guo, J.-F. Du, D.-S. Chen, P. Chen, H.-Z. Xing, *Dalton Trans.* **2018**, 47, 909–915.
- [20] T. Kajiwara, M. Fujii, M. Tsujimoto, K. Kobayashi, M. Higuchi, K. Tanaka, S. Kitagawa, *Angew. Chem. Int. Ed.* **2016**, 55, 2697-2700.